Journal of Applied Polymer Science

Insights into process–structure–property relationships of poly(ethylene terephthalate) industrial yarns by synchrotron radiation WAXD and SAXS

Yatao Liu,[1] Lixin Yin,[2] Huirong Zhao,[2] Guangkun Song,[2] Fangming Tang,[2] Lili Wang,[2] Huili Shao,[1] Yaopeng Zhang[1]

[1]State Key Laboratory for Modification of Chemical Fibers and Polymer Materials, College of Materials Science and Engineering, Donghua University, Shanghai 201620, China

[2]Jiangsu Hengli Chemical Fibre Co., Ltd., Wujiang, Jiangsu Province 215228, China

Correspondence to: Y. Zhang (E-mail: zyp@dhu.edu.cn)

ABSTRACT: Synchrotron radiation wide angle X-ray diffraction (WAXD) and small angle X-ray scattering (SAXS) were performed to study the structures of four typical types of poly(ethylene terephthalate) (PET) industrial yarns. Three-dimensional structural models of the yarns and comprehensive insights into the process–structure–property relationships were gained. High spinning speed, low draw ratio, and high heat-setting temperatures lead to HMLS yarns with high crystallinity, high amorphous orientation, densely packed lamellar stacks, and a small tilting angle of crystalline lamellae. High draw ratio tends to result in PET industrial yarns with large long period and a large tilting angle of lamellae. Heat-setting process has a significant influence on the amorphous orientation and crystalline structures, such as crystallinity, crystallite size, as well as crystal grain number. Compared with other structure characteristics, amorphous orientation plays a more important role in determining the tenacity, initial modulus, part load elongation, ultimate elongation, as well as shrinkage of PET industrial yarns. The crystal grain number seems to have an effect on the initial modulus, while the long period influences the elongation of the yarns to some extent. In addition, the small tilting angle of crystalline lamellae may relate to the dimensional stability of PET yarns. © 2015 Wiley Periodicals, Inc. J. Appl. Polym. Sci. **2015**, *132*, 42512.

KEYWORDS: crystallization; fibers; structure–property relations; supramolecular structures; X-ray

Received 21 January 2015; accepted 18 May 2015

DOI: 10.1002/app.42512

INTRODUCTION

Poly(ethylene terephthalate) (PET) is a thermoplastic polymer with excellent properties and has attracted many researchers' attention because of its large number of applications in the form of plastic, film, and fiber.[1–23] A thorough understanding of the structures of PET is of great interest. For example, Cruz *et al.*[5] investigated the structures of PET crystallized at different temperatures. Stribeck *et al.*[10] studied the structures of high-pressure crystallized PET utilizing the interface distribution function (IDF). Shioya *et al.* conducted a detail investigation on the long-period structures forming bundles of PET fibers.[15]

In the applications of PET, the form of fiber is of great demand and considerable commercial importance. Over the past decades of years, PET industrial yarns have been widely used in many fields such as reinforcement in passenger radial tires, seat belts, coated fabrics, geotextiles, ropes, and cordage, due to its high tenacity, high modulus, and low shrinkage.[23,24] Numerous attempts have been made to explain the structure–property relationships of PET fibers.[1,3,4,9,18,19,23–30] These attempts can be classified in four categories, i.e., characterization of the semi-crystalline structure and morphology, the effect of process conditions on the structures and properties, the influence of heat setting on the morphology and properties and the *in situ* studies on the structure formation. For instance, Hsieh *et al.* and Youssefi *et al.* studied the crystalline structures of PET fibers, respectively.[3,18] Hirahata *et al.* conducted an online measurements of orientation induced crystallization of PET during high speed spinning by means of synchrotron radiation wide angle X-ray diffraction (WAXD).[7] Gputa *et al.*, Chao *et al.*, and Wang *et al.* studied the effect of heat treatment on the structures and properties of PET fibers, respectively.[1,2,25,27,31,32] Shioya *et al.* conducted a study on tensile fracture process of PET fibers using time-resolved small angle X-ray scattering (SAXS).[19]

Additional Supporting Information may be found in the online version of this article.

It is known that PET is a semicrystalline polymer and forms a triclinic crystallite. In general, PET consists of two phases, the crystalline phase and the amorphous phase. However, many studies have revealed that the amorphous phase consists of two fractions, mobile amorphous fraction (MAF) and rigid amorphous fraction (RAF) in these years. RAF has partial order and is located between the MAF and the crystalline regions.[33] In addition, there exist other structure models of PET like dual lamellar stack models (with primary and secondary stacks).[34,35] For PET fibers, two-phase model consisting crystalline and amorphous phase was generally used to analyze the structures by many researchers.[4,23,24,30,36] In this model, fibrils are the fundamental building blocks and are made of lamellar stacks along the fiber axis. The ordered (crystalline) regions alternate with less ordered (amorphous) domains, forming the lamellar stacks. The molecules running through several crystalline and amorphous regions are the so-called "tie molecules". There is also the possibility that a molecule folds back on the surface of a crystal to reenter it. The polymer molecules are oriented along the fiber axis depending on the process conditions. Extended noncrystalline molecules are dispersed in the fibrils. Besides crystalline and amorphous phase, some researchers proposed a third phase, an oriented, intermediate phase, located mainly between the fibrils, to correlate fiber structures and properties.[37] In this paper, the classical two-phase model remained the foundation of the present work.

In the course of manufacture, a set of process condition parameters, such as spinning speed, draw ratio, and heat setting, are applied to produce yarns with specific structures and mechanical properties. Huisman *et al.*[4] studied the effect of spinning speed and drawing temperature on the structures and properties of PET yarns. It was found that the hot air shrinkage decreased with spinning speed and was controlled by amorphous orientation as well as the fraction of amorphous regions. A useful parameter related to both crystalline and amorphous regions was established to describe the modulus. Abbasi *et al.*[38] reported the effect of spinning speed on the structure and physical properties of yarns produced from used PET bottles. It was found that increasing the take-up speed (from 2500 to 3000 m/min) resulted in an increase in the optical birefringence, crystallinity, tenacity, and initial modulus and a reduction in the breaking elongation of both virgin and used samples. Kolb *et al.*[39] conducted an investigation on the high speed spinning process of PET fibers by means of synchrotron WAXD. Results showed that necking and crystallization were closely coupled, and no orientation of amorphous matrix prior to crystallization could be detected. Cho *et al.*[31] studied the formation of microcrystals in PET fibers. Results showed that the PET molecules were relaxed and became crystallized during a short heat treatment at 190°C for 1.2 s. In addition, previous studies on structure-property relationship of PET yarns have revealed that the amorphous phase is of great importance in affecting the properties.[9,23,24,40] Rim *et al.* and Samui *et al.* investigated the property and morphology of different types of PET yarns and found that tenacity, shrinkage and initial modulus are primarily controlled by amorphous orientation.[23,24] Murthy *et al.* thought that other factors (not amorphous orientation) such as the connectivity between the amorphous phase and the crystalline regions play an important role in determining the tenacity of the fibers.[9] While Peng *et al.* indicated that PET fibers obtained by high speed spinning possess a more compliant interfibrillar amorphous phase, which may account for both the greater dimensional stability, as well as the more reversible mechanical behavior.[40] Murthy *et al.* investigated the structure changes of PET fibers as a function of applied stress.[30] It was found that tenacity and dimensional stability are mainly determined by the diameter of lamellar stacks, tilting angle of the lamellae, and the strain in the lamellar spacing. Modulus at low elongation and ultimate elongation are determined by the long-spacing strain.

These previous studies have provided us abundant and valuable knowledge about PET fibers. However, there are still some limitations on the exploration of structure-property relationship of PET fibers. Some researchers focused on the amorphous phase and ignored the influence of crystalline domains on the mechanical properties.[23,24] Some stressed the importance of crystalline structures and did not pay enough attention to the amorphous regions.[26] Moreover, detailed information about how process conditions such as spinning speed, draw ratio and heat-setting temperatures, affect the fiber structures and properties were not involved in the previous studies. Samui *et al.* paid much attention to the influence of amorphous regions on the fiber properties, yet the process conditions, structures derived from SAXS were not considered into the studies.[23] Thus, a comprehensive understanding of the process–structure–property relationships on PET industrial yarns was still not given.

In this paper, we re-examined the hierarchical structures of various structural elements of four typical PET industrial yarns with different process conditions and mechanical properties, mainly using synchrotron radiation WAXD and SAXS. WAXD was used to characterize the structures in the crystalline scale while SAXS was used to detect the structures at fibrillar length scale. The main objective of this paper is to present a comprehensive understanding of the process–structure–property relationships and provide theoretical direction to produce new types of polyester fibers with desired properties.

EXPERIMENTAL

Materials

PET industrial yarns were produced by Hengli Corporation and were designated as high modulus and low shrinkage (HMLS) yarn, high tenacity (HT) yarn, low shrinkage (LS) yarn and super low shrinkage (SLS) yarn. The lot number and specifications of the four yarns are HM 100 (1000 D/336 f), HT 116 (1000 D/192 f), LS 105 (1000 D/192 f), and SLS 120 (1000 D/192 f), respectively.

HMLS yarn was produced at high spinning speed, low draw ratio, and high heat-setting temperatures while LS and SLS yarns were produced at low spinning speed, high draw ratio and high heat-setting temperatures. HT yarn was produced at low spinning speed, high draw ratio, and low heat-setting temperatures. The heat-setting temperatures of SLS yarn are higher than those of LS yarn. For the purpose of technology confidentiality, the general ranges instead of the accurate value of the

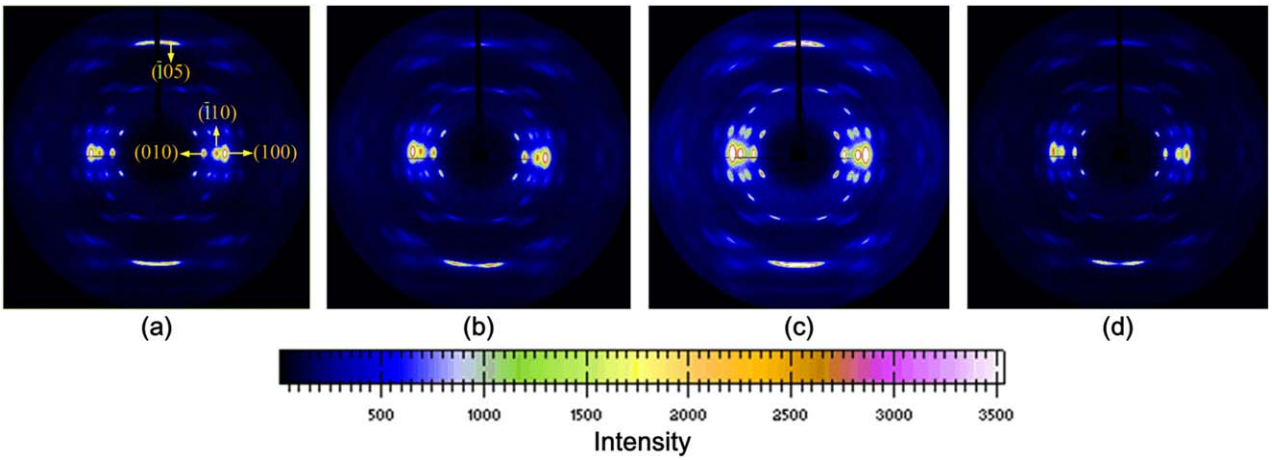

Figure 1. Two-dimensional WAXD patterns of (a) HMLS, (b) HT, (c) LS, and (d) SLS yarns. [Color figure can be viewed in the online issue, which is available at wileyonlinelibrary.com.]

process condition parameters were shown. The spinning speed ranges from 500 to 2500 mm/min, while draw ratio ranges from 1.5 to 6.5. The heat-setting temperatures range from 150 to 250°C and the time held at heat-setting process is within 10^{-2} s.

Characterizations

Mechanical and Shrinkage Measurements. Tensile measurements were performed using an Instron 5969 (gauge length: 500 mm; cross-head speed: 500 mm/min). Shrinkage was determined on a Lenzing TST10 Instruments made in Austria. HMLS, HT, LS, and SLS yarns were measured at 177°C under 0.05 cN/dtex for 10 min.

WAXD. WAXD was carried out at BL15U1 in Shanghai Synchrotron Radiation Facility (SSRF). The energy of the X-ray radiation was 20 keV and the wavelength of this beamline was 0.6199 Å. The yarns were vertically mounted in a custom-built sample holder. The acquisition time for WAXD measurements were 5 s. The WAXD patterns were recorded with a two-dimensional MarCCD detector. The sample-to-detector distance and the size of the beamspot were 191 mm and 3 × 2 μm, respectively. The diffraction angle was calibrated using CeO_2 from SSRF. All data were corrected for background scattering before analysis and treated with a software of Fit2D.

The one-dimensional equatorial WAXD diffractograms were analyzed by curve-fitting procedures to separate crystalline diffractions from amorphous scattering to obtain crystallinity and crystallite sizes using Peakfit V4.12 software. The bell-shaped function used in the fitting procedure is a Pearson VII function.[4,41] The relative crystallinity index (X_c) was determined by the ratio of the integrated intensity of crystalline peaks and the entire equatorial scattering intensity.[29] Because of disorder effect and truncation effect, the integrated diffraction intensity is just an estimate. Moreover, intensity in reciprocal space and density fluctuation in real space are not simply related by linear relation. Thus, the crystallinity in this study is just a relative crystallinity index. As only a relative structure-property relationship is of interest, the more precise techniques calculating the crystallinity were not used in this paper.[42–44] Since the equatorial reflections were used to determine the crystallinity index, it is more accurate to label the relative crystallinity index as "X_c equatorial". Lateral crystallite sizes were determined from the equatorial planes (010), (1̄10), and (100), and longitude crystallite size was estimated from the nearly meridian plane (1̄05). Crystallite size ($D_{(hkl)}$) was calculated according to the Scherrer equation.[23,45] Crystal grain volume (V_c) was calculated according to Kiang's method.[41] Hermans crystallite orientation factor (f_c) was determined from the azimuthal scan of three equatorial planes *viz.* (010), (1̄10), and (100) according to Gupta's method.[46]

SAXS. SAXS was carried out at BL16B1 in SSRF. The energy of the X-ray radiation was 10 keV, resulting in a wavelength of 1.24 Å. The yarns were vertically mounted in a custom-built sample holder. The acquisition time for SAXS measurements were 8 s and the SAXS patterns were recorded with a two-dimensional MarCCD detector. The sample-to-detector distance was 1940 mm and the size of the beamspot was 1 × 1 mm. The effective scattering vector $h\,(h{=}4\pi\sin\theta/\lambda)$ (where 2θ is the scattering angle, and λ is the wavelength of X-ray) lies in the range 0.07–2.2/nm. The scattering angle was calibrated using chicken collagen standard from SSRF. All data were corrected for background scattering before analysis and treated with the software Fit2D.

In the SAXS patterns, the scattering vectors along and perpendicular to the fiber axis are defined as h_1 and h_2, respectively. The one-dimensional scattering spectra $I(h_1)$ along the fiber axis can be obtained by considering the scattering intensity distribution along the h_1 direction, which was obtained by meridian scans along h_1 for certain intervals of h_2 as schematically shown in the top left corner of Figure 4. The long period along the fiber axis can be obtained according to the Bragg's law.[30] The average thickness of the crystalline and amorphous regions along the fiber axis can be derived from the one-dimensional correlation function of the distribution of the electron density in the lamellar stacks $K(Z)$ as the following equation:[47–50]

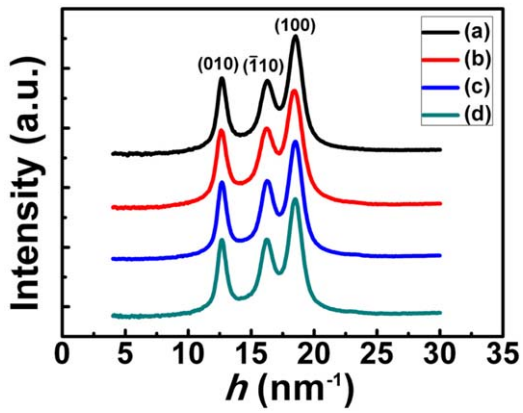

Figure 2. One-dimensional equatorial WAXD diffractograms of (a) HMLS, (b) HT, (c) LS, and (d) SLS yarns. [Color figure can be viewed in the online issue, which is available at wileyonlinelibrary.com.]

$$K(Z)=\frac{\int_0^\infty I(h_1)\cos(h_1 Z)\mathrm{d}h_1}{\int_0^\infty I(h_1)\mathrm{d}h_1} \quad (1)$$

where Z is the fiber axis direction. The Lorentz correction where $I(h)$ is multiplied by h^2 is not applied because of the anisotropic orientation of the lamellae in the highly oriented PET industrial yarns.[47,51] Detailed analysis method of WAXD and SAXS can be found in the Supporting Information. The lamellar thickness derived from eq. (1) is not accurate because the first minimum in reality never reach horizontal zone, and the initial slope can never be accurate for this kind of sample with considerable amount of defect (disorder effect). The one-dimensional correlation function used in this paper is a relatively simple and practicable method to derive the general structural differences of the four yarns. Additionally, it is necessary to note that there exists a more precise Chord distribution function (CDF) developed by Stribeck to characterize samples with fiber symmetry.[52,53]

Density Measurements. Densities of HMLS, HT, LS, and SLS yarns were measured on a solid density instrument (UL Trapycnometer 1000) at 25°C.

Sonic Measurements. Sonic measurements were made on a digital fiber sound velocimeter (SCY-III) designed by Donghua University. Sonic orientation was calculated according to Moseley's method.[54] Sonic modulus was calculated according to Dumbleton's method.[55] The amorphous orientation was determined according to the two-phase sonic modulus theory proposed by Samuels.[56]

RESULTS AND DISCUSSION

Structures from WAXD Results

The typical two-dimensional WAXD patterns of HMLS, HT, LS, and SLS yarns are presented in Figure 1. The patterns show the characteristic diffraction spots of (010), ($\bar{1}$10), and (100) lattice planes along the equator and the ($\bar{1}$05) lattice plane near the meridian.

Figure 2 shows the one-dimensional equatorial WAXD diffractograms of all the four yarns, from which we can get the crystalline structural information through "deconvolution" technique (Supporting Information Figure S1). The detailed crystalline structural parameters are summarized in Table I. V_c is the average volume of crystal grains and the estimated number of crystal grains per cubic centimeter is given by the relation $N=(X_c/V_c)\times 10^{21}$. Crystallinity of HMLS yarn and SLS yarn was measured to be around 60%, whereas LS yarn has relatively lower crystallinity and HT yarn has the lowest crystallinity. The order of crystallite size and crystal volume is SLS > LS > HMLS > HT. WAXD data indicate that the crystalline structure of HMLS yarn is much different from the other three yarns. HMLS yarn has relatively smaller crystal grain sizes, the highest crystallinity, the highest crystallite orientation factor (f_c), and the largest crystal grain number, indicating a more compact structure of the HMLS yarn.

The differences in crystallinity, crystallite size, and number of crystal grains are mainly caused by the heat-setting process. Amorphous molecules in the heat-setting process have sufficient mobility and are able to become crystallized to some extent, which contribute to the higher crystallinity and larger crystallite size. Furthermore, high temperatures (near melting point T_m) are likely to cause the melting of small crystal grains, resulting in the reduction of crystal grain number. Therefore, LS and SLS yarns have higher crystallinity, larger crystallite size, as well as less crystal grains than HT yarn. As for HMLS yarn, molecules at high spinning speed tend to orient more along the fiber axis. The high molecular orientation promotes the crystallization rate and results in more crystal nuclei. This is why HMLS yarn has more crystal grains than LS and SLS yarn.

Sonic Orientation and Amorphous Orientation

The results of sonic and density measurements are shown in Table II. The densities (ρ) of the yarns in this work were obtained using a solid density instrument, which was different

Table I. Structural Parameters of HMLS, HT, LS, and SLS Yarns by WAXD

			Crystallite size (Å)					
Yarns	X_c (%)	f_c	$D_{(010)}$	$D_{(\bar{1}10)}$	$D_{(100)}$	$D_{(\bar{1}05)}$	V_c (nm^3)	N (10^{18}/cm^3)
HMLS	60.4	0.987	62	56	46	81	176	3.7
HT	54.5	0.978	58	48	43	79	147	3.4
LS	57.5	0.978	67	56	47	83	197	2.9
SLS	60.7	0.979	67	60	48	83	201	3.0

X_c relative equatorial crystallinity index, f_c Hermans crystallite orientation factor, V_c crystal grain volume, N crystal grain number per cubic centimeter.

Table II. Density, Sonic Modulus, Sonic Orientation, and Amorphous Orientation of HMLS, HT, LS, and SLS Yarns

Yarns	ρ (g/cm^3)	E_{or} (GPa)	f_s	f_a
HMLS	1.3610	31.49	0.921	0.791
HT	1.3568	38.55	0.936	0.857
LS	1.3600	24.57	0.899	0.753
SLS	1.3633	22.25	0.888	0.704

ρ density, E_{or} sonic modulus, f_s sonic orientation, f_a amorphous orientation.

from the traditional density gradient method. Therefore, the numerical value of the density is a little bit smaller than that in the previous studies.[24] E_{or} is the sonic modulus in the orientation direction of the yarns. The sonic orientation parameter (f_s) calculated from sound velocity relates to the total molecular orientation and is a measure of the average orientation of all molecules in the yarn regardless of the degree of crystallinity.[54] Compared with other yarns, HT yarn has the highest sonic modulus and total molecular orientation, indicating that the degree of the overall molecules order is the highest. HMLS yarn possesses relatively higher sonic modulus and total molecular orientation than LS and SLS yarns. Amorphous orientation (f_a) is a very important structural parameter related to fiber properties. As presented in Table II, HT yarn has the highest amorphous orientation, while SLS yarn has the lowest amorphous orientation. In addition, the results suggest that a yarn with high amorphous orientation (f_a) also has high total molecular orientation (f_s).

In the course of fiber manufacture, drawing and heat-setting process have opposite influence on molecular orientation. Drawing increases the molecular orientation whereas heat-setting decreases the orientation. Given the fact that HT, LS, and SLS yarns have similar spinning speed and draw ratio, it is reasonable to conclude that the orientation (f_a and f_s) differences are mainly caused by the heat-setting process. In addition, the higher orientation (f_a and f_s) of HMLS yarn than LS and SLS yarns is attributed to the high spinning speed of HMLS yarn.

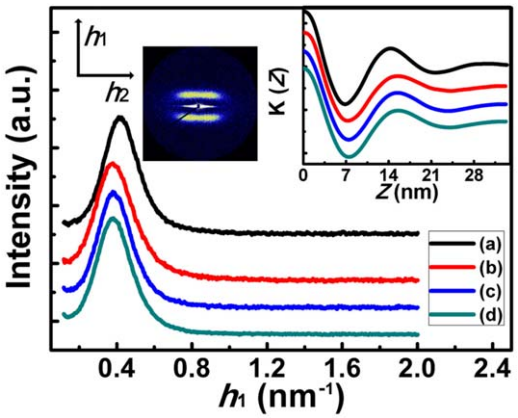

Figure 4. One-dimensional SAXS profiles along h_1 of (a) HMLS, (b) HT, (c) LS, and (d) SLS yarns. The insets show (left) the scattering vectors along and perpendicular to the fiber axis, h_1 and h_2, and (right) the one-dimensional electron density correlation function. Curves were shifted vertically for sake of clarity. [Color figure can be viewed in the online issue, which is available at wileyonlinelibrary.com.]

Structures from SAXS Results

SAXS is very suitable to characterize the structure features on a long distance scale (1 nm–0.1 μm). Typical two-dimensional SAXS patterns of all the four yarns are shown in Figure 3. There are two important features in a two-dimensional SAXS pattern, the diffuse scattering near the beam spot and the lamellar peaks in the meridian direction.[30] In this study, we mainly focus on the lamellar peaks, which are the contributions of lamellae along the fiber axis.

The SAXS patterns reveal that the lamellar stacks exist in the fiber structure. Figure 4 shows the one-dimensional profiles of $I(h_1)$ of the four yarns. Long period (L) implies the repeat unit distance of crystalline and amorphous phase in the fiber structure. The peak maximum at around 0.4/nm was used to

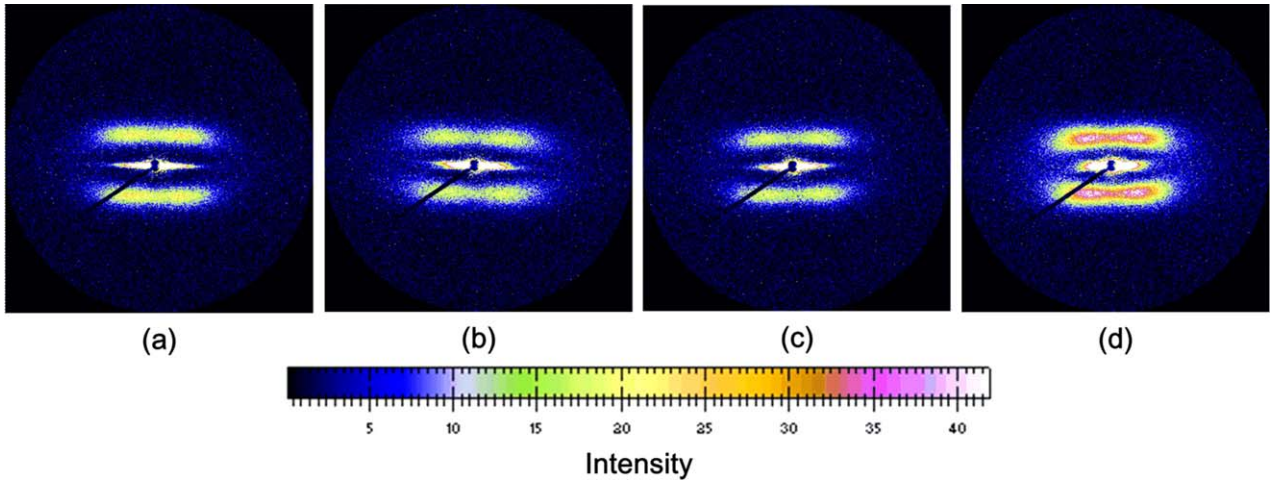

Figure 3. Two-dimensional SAXS patterns of (a) HMLS, (b) HT, (c) LS, and (d) SLS yarns. [Color figure can be viewed in the online issue, which is available at wileyonlinelibrary.com.]

Table III. Structural Parameters of HMLS, HT, LS, and SLS Yarns by SAXS

Yarns	L (nm)	L^*(nm)	L_c (nm)	L_a (nm)	X_L (%)	Φ (°)
HMLS	15.30	14.32	9.08	5.24	63.4	42.6
HT	16.66	15.52	10.13	5.39	65.3	50.3
LS	16.48	15.45	9.68	5.77	62.6	47.6
SLS	16.60	15.50	9.80	5.76	63.0	45.0

L-long period derived from the Bragg's law, L^*-long period derived from the one-dimensional correlation function, X_L = linear crystallinity, X_L-L_c/L^*, L_c-thickness of crystalline regions, L_a-thickness of amorphous domains, Φ-the angle between the normal to the lamellar surface and the fiber axis.

determine the long period along the fiber axis and the results are shown in Table III. Generally, the fiber with large long period means that the lamellar stacks are loosely packed. HT yarn has the largest long period while HMLS yarn has the smallest one. Compared with the other three yarns, HMLS yarn has more compactly packed lamellar stacks.

In order to obtain detailed information about the average thickness of the amorphous and crystalline regions, the one-dimensional electron density correlation function (Figure 4) was adopted to analyze the one-dimensional scattering profiles $I(h_1)$. The long period calculated by Bragg's law is larger than that calculated from the correlation function, which has been reported by previous studies.[48] The specific structural parameters derived from correlation function are presented in Table III. HT yarn has the largest crystalline lamellar thickness (L_c) while HMLS, LS, and SLS yarns have smaller L_c. It is possible for us to understand the distribution of crystalline lamellae and amorphous domain along the fiber axis through the linear crystallinity (X_L).[24,47] Due to the extended noncrystalline molecules or interfibrillar amorphous regions between the lamellar stacks, the X_L is higher than the crystallinity (X_c) obtained from WAXD.[24,30] Since HT yarn possesses the largest linear crystallinity from SAXS and the smallest crystallinity index from WAXD, it seems plausible that HT yarn has more interfibrillar amorphous regions than the other three yarns. Others have also discussed the importance of such a phase.[37]

In SAXS patterns of PET industrial yarns and some other highly oriented semicrystalline polymers, the lamellar peak often appears as a bar and may be a coexistence of two-point and four-point patterns.[30] When the lamellar surface is perpendicular to the chain axis, a two-point pattern appears. When the lamellar surface is tilting away from the chain axis, a four-point pattern emerges.[57] Figure 5 shows the azimuthal scans of the lamellar peaks along h_2 of the four yarns. The curves were fitted with two Pearson VII functions, shown in the right inset of Figure 5. The tilting angle (Φ) between the normal of the lamellae and the fiber axis was calculated according to the following equation:[47]

$$\Phi = \tan^{-1}\frac{\Delta\chi}{2h_{1,\max}} \quad (2)$$

where $h_{1,\max}$ is the lamellar peak position along the meridian direction and $\Delta\chi$ is the separation of the centers of the two Pearson VII functions. Because of symmetry, there are four peak maximums in a SAXS pattern. Considering the relatively large distance between the two Pearson VII peaks and the deconvolution results, we regard the SAXS patterns of PET yarns as four-point patterns rather than two-point patterns. The tilting angles (Φ) of the four yarns are shown in Table III. Among the four yarns, HMLS yarn has the smallest tilting angle and HT yarn has the largest tilting angle.

The structure differences derived from SAXS data are controlled by the process conditions. Our data indicated that low spinning speed and high draw ratio are expected to produce yarns with large long period and large tilting angle of crystalline lamellae, and vice versa. According to Murthy's previous study, the lamellae are frozen in the final orientation with a small tilting angle when fibers are spun at high speeds.[30] High draw ratios will distort the lamellae and increase the tilting angle.

Mechanical Properties and Shrinkage

Mechanical response of the yarns on loading is the reflection of the fiber structures. Tensile properties and shrinkage of HMLS, HT, LS and SLS yarns are summarized in Table IV. HT yarn has the highest tenacity and the largest shrinkage. HMLS yarn has the highest initial modulus, the smallest part load elongation and ultimate elongation. SLS yarn has the smallest shrinkage as well as the largest ultimate elongation and part load elongation. Dimensional stability is the sum of part load elongation and shrinkage. HMLS yarn shows the smallest value of dimensional stability, indicating the best dimensional stability.

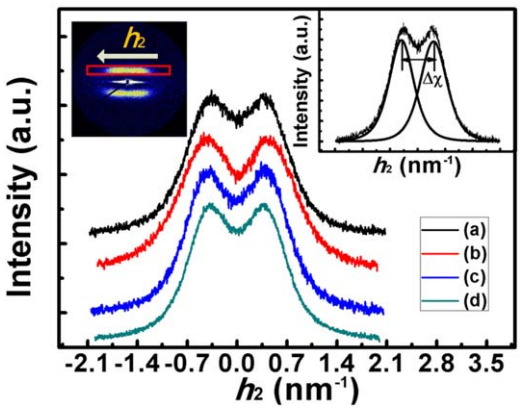

Figure 5. Azimuthal scan of the lamellar peaks along h_2 of (a) HMLS, (b) HT, (c) LS, and (d) SLS yarns. The insets show (left) the integrating area along h_2 and (right) the fit procedure for the tilting angle of the lamellae. [Color figure can be viewed in the online issue, which is available at wileyonlinelibrary.com.]

Table IV. Mechanical Properties and Shrinkage of HMLS, HT, LS, and SLS Yarns

Properties	HMLS	HT	LS	SLS
Tenacity (cN/dtex)	7.5	8.3	7.4	7.3
Initial modulus (cN/dtex)	99.4	96.2	88.5	84.2
Part load elongation (PLE %)	5.0	6.1	11.0	12.9
Ultimate elongation (UE %)	12	14.1	18.5	21.1
Shrinkage (%)	3.50	5.67	1.47	0.89
Dimensional stability	8.50	11.67	12.47	13.79

Decitex (also Dtex) is a unit traditionally used in textile industry to measure the linear density of a single fiber of yarn. One dtex equals a density of one gram per 10 km of length. Tenacity is breaking stress in the tensile process, while initial modulus is the first maximum in the modulus–strain curves. PLE indicates elongation of the yarn at specific load (4 cN/dtex). UE is the breaking elongation of the yarn. Shrinkage refers to the degree of fiber shrinkage at specific conditions (at 177°C under 0.05 cN/dtex for 10 min). Dimensional stability is the sum of part load elongation and shrinkage.

Representative stress–strain curves and modulus–strain curves are depicted in Figure 6. HMLS and HT yarns have higher initial modulus and lower elongation while LS and SLS yarns have lower initial modulus and higher elongation. Lv *et al.* studied the modulus–strain curves of PET industrial yarns and found that the modulus–strain curves can be divided into three stages.[13] The tensile behaviors of the four yarns in our work are consistent with Lv's findings. The first stage is from the beginning to the first modulus peak, which is associated with amorphous regions. The first modulus peak appears at around 0.4% strain. The second stage is from the first peak to the second peak. In this stage, the crimpled molecules begin to uncoil. The second maximum of the modulus of HMLS and HT yarns appears at lower strain than that of LS and LS yarns. This phenomenon is caused by the molecular orientation. Since HMLS and HT yarns have higher amorphous orientation, the coiled amorphous molecules have less possibility to extent in a large scale. The third stage is from the second peak to the rupture of the yarn. The crystalline regions start to slip until some molecular rupture is formed in the amorphous domains.

Three-Dimensional Structural Models and Process–Structure–Property Relationships of PET Industrial Yarns

Based on the WAXD, SAXS, sonic, and density measurements, we proposed straightforward three-dimensional structural models of our HMLS, HT, LS, and SLS yarns (Figure 7). In these models, the shapes of the crystalline lamellae are simplized as cuboids. The lateral dimensions of the crystalline lamellae are estimated as the average of the three equator crystallite sizes $(D(010) + D(\bar{1}10) + D(100))/3$. It is necessary to note that the models in this study are just to show the structure characteristics like crystallite size, crystal grain volume, amorphous orientation, long period, thickness of amorphous and crystalline regions and the lamellae tilting angle. In fact, they are not comprehensive models for the fiber structures are very complicated.

Generally, fiber structures are determined by a set of spinning and drawing conditions that are unique for different types of industrial yarns. High spinning speed results in more crystal nuclei, higher molecular orientation and smaller tilting angle of crystalline lamellae. And the precursor structure has limited change during the subsequent drawing and heat-setting process, which can be proved from the high crystallite and amorphous orientation, and a large number of small crystal grains of HMLS yarn. Drawing process leads to high orientation and large tilting angle of crystalline lamellae. High temperature (near T_m) not only induces the coiling of amorphous molecules, but also causes the melting of small crystal grain and the crystallization of amorphous molecules. As a result, heat-setting process leads to the reduction of amorphous orientation and crystal grain as well as the increase of crystallinity. The relationships between yarn structures and properties are discussed below.

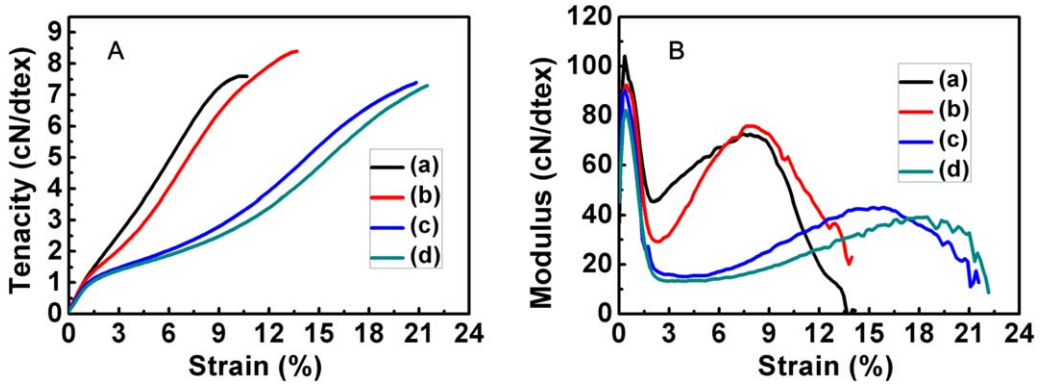

Figure 6. (A) Stress–strain curves and (B) modulus–strain curves of (a) HMLS, (b) HT, (c) LS, and (d) SLS yarns. [Color figure can be viewed in the online issue, which is available at wileyonlinelibrary.com.]

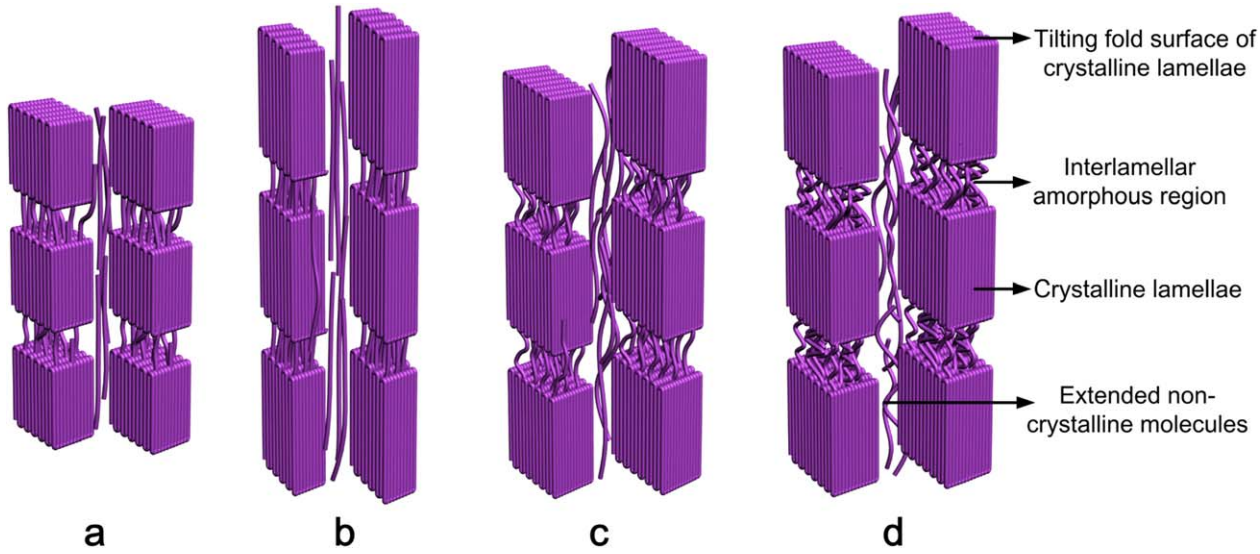

Figure 7. Three-dimensional structural models of (a) HMLS, (b) HT, (c) LS, and (d) SLS yarns. [Color figure can be viewed in the online issue, which is available at wileyonlinelibrary.com.]

Tenacity. Tenacity is one of the most important mechanical properties of PET industrial yarns. Previous studies have proved that amorphous phase is of significance in affecting tenacity.[4,9,23,24] From the sonic and mechanical measurements, we learn that HT yarn has the highest amorphous orientation and tenacity while SLS yarn has the lowest amorphous orientation and tenacity. As shown in Figure 8(a), amorphous orientation correlates well with tenacity, which is consistent with some previous studies.[23,24] It may be inferred that yarns with high amorphous orientation possess high tenacity, and amorphous orientation seems to be the key structural parameter in determining yarn tenacity. In addition, it is necessary to point out that others have discussed the role of the connectivity between the amorphous phase and crystalline regions in affecting the tenacity of PET fibers.[9,30]

Modulus. Another important property of PET industrial yarns is the initial modulus. Previous studies have revealed that initial modulus is primarily controlled by amorphous orientation.[23,24] Huisman used the overall orientation factor consisting of both the crystalline and amorphous orientation to describe the initial modulus.[4] Cho found that the microcrystals in the amorphous regions affect the initial modulus of PET fibers.[31] Others also argued the importance of "tie molecules".[13,58] Actually, the modulus maximum occurs at the first stage during the tensile process, which is mainly associated with the amorphous regions. The correlation between amorphous orientation and initial modulus is illustrated in Figure 8(b). Overall, with increased amorphous orientation, the value of initial modulus rise. Interestingly, the orientation of HMLS yarn is lower than that of HT yarn, but the initial modulus of HMLS yarn is higher than that of HT yarn. It can be learnt from Cho's study that the microcrystals in the amorphous regions affect the initial modulus of PET fibers. WAXD results indicate that HMLS yarn possesses a large number of small crystal grains. Therefore, it seems reasonable to attribute the higher initial modulus of HMLS yarn than HT yarn to these small crystal grains. More crystal grains indicate a larger surface area and large interdomain linkages, which may contribute to the high initial modulus of PET yarns to some extent.

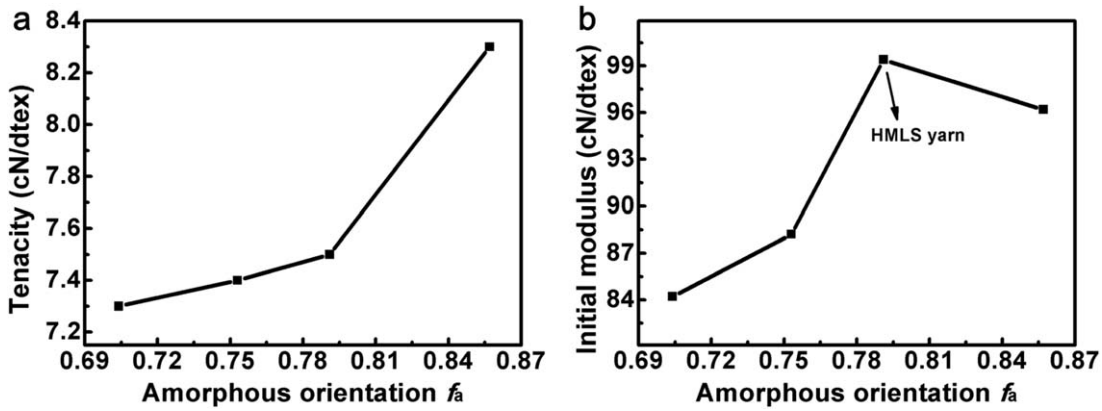

Figure 8. (a) Correlation between amorphous orientation and tenacity. (b) Correlation between amorphous orientation and initial modulus.

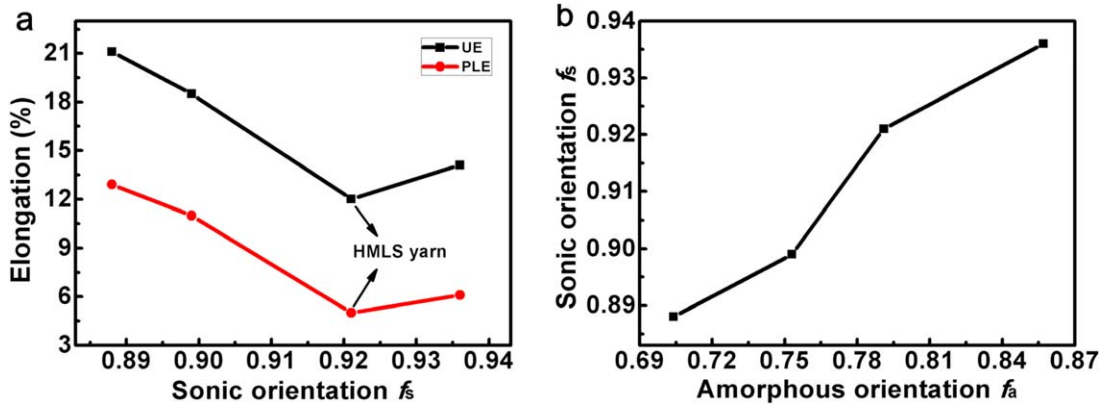

Figure 9. (a) Correlation between sonic orientation and part load elongation (PLE) and ultimate elongation (UE). (b) Correlation between amorphous orientation and sonic orientation. [Color figure can be viewed in the online issue, which is available at wileyonlinelibrary.com.]

Elongation. Since both the crystalline and amorphous regions are involved during the tensile deformation, the ultimate elongation is mainly governed by the sonic orientation (total molecular orientation). SLS and LS yarns have the lowest total molecular orientation, indicating that the coiled molecules are possible to stretch to a larger extent than HMLS and HT yarns. Consequently, LS and SLS yarns have larger ultimate elongation. This can be confirmed from the relationship between the sonic orientation (f_s) and ultimate elongation in Figure 9(a). The ultimate elongation decreases with increasing sonic orientation (f_s). However, HMLS yarn is not perfectly consistent with this relationship. Although the sonic orientation of HT yarn is higher than HMLS yarn, the elongation of HT yarn is larger than HMLS yarn. The smaller elongation of the HMLS yarn may be caused by densely packed interlamellar spaces that can be known from the smaller long period of the HMLS yarn [Figure 7(a)].[30] Similarly, part load elongation is also determined by the sonic orientation, shown in Figure 9(a).

Figure 9(b) shows the relationship between amorphous orientation and sonic orientation. It is evident that the sonic orientation increases with the increasing amorphous orientation. Since the four PET yarns have comparable crystallite orientation and different amorphous orientation, the sonic orientation is mainly controlled by the amorphous orientation. In other words, it can be concluded that the amorphous orientation is the key structure characteristic in influencing the elongation of PET yarns.

Shrinkage. As shrinkage is a highly relevant characteristic of PET industrial yarns, it seems necessary to point out how shrinkage is determined in terms of structural parameters. The driving force behind shrinkage is of entropic nature. Some researchers have revealed that shrinkage is highly governed by the amorphous regions.[9,23,24,30] At high temperatures (177°C), extended molecules in amorphous regions have sufficient mobility to obtain their most probable configuration, meaning these molecules are likely to coil up and shrink largely. In contrary, the crystalline phase may be regarded to behave as rigid and state blocks and do not contribute to the thermal shrinkage. Therefore, the thermal shrinkage is mainly determined by the amorphous regions. The simple models in Figure 7 show the coiled amorphous molecules and rigid crystalline phase clearly. The correlation between amorphous orientation and shrinkage in this study is depicted in Figure 10(a). Low amorphous orientation leads to small shrinkage, and vice versa. As illustrated in Figure 7(d), SLS yarn has the minimum amorphous orientation and therefore having the lowest shrinkage amongst the four yarns. Besides amorphous orientation, Huisman thought that

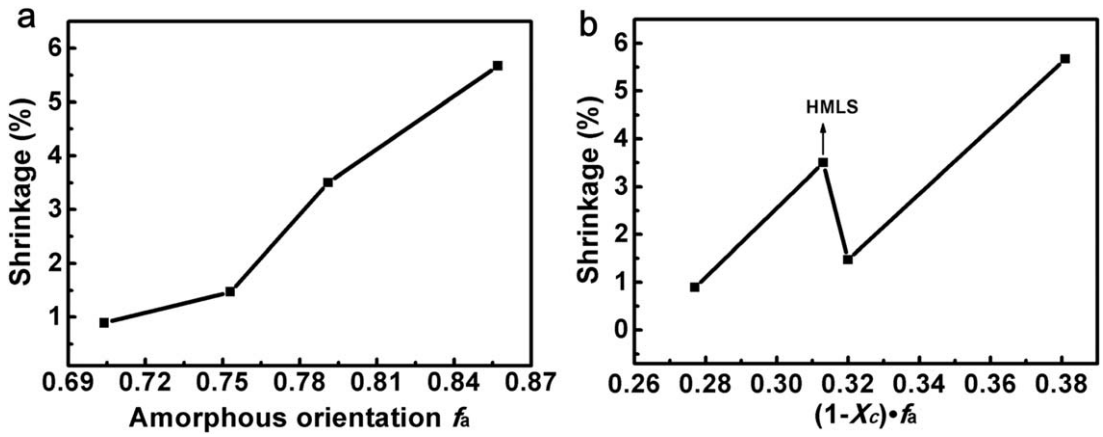

Figure 10. (a) Correlation between amorphous orientation and shrinkage. (b) Correlation between structural parameters $(1 - X_c)\cdot f_a$ and shrinkage.

Table V. A Brief Summary of Process–Structure–Property Relationships of PET Industrial Yarns

Structural parameters	Mainly related processing conditions	Related properties
Amorphous orientation (f_a)	Spinning speed, draw ratio, heat-setting temperature	Tenacity, initial modulus, part load elongation, ultimate elongation, shrinkage
Crystal grain number (N)	Spinning speed, heat-setting temperature	Initial modulus
Long period (L)	Spinning speed, draw ratio	Part load elongation, ultimate elongation
Tilting angle (Φ)	Spinning speed, draw ratio	Dimensional stability

the fraction of amorphous phase also matters the shrinkage behavior and more amorphous phase induces more thermal shrinkage.[4] A useful structural parameter $(1 - X_c)f_a$ was established in his studies to describe the shrinkage behavior of PET fibers. Figure 10(b) illustrates the plot of shrinkage and the value of $(1 - X_c)f_a$. From this plot, it is clear that an approximate correlation appears, however, the four yarns do not fit this correlation very well. This may be caused by a lack of sample data. Furthermore, note that the crystallinity of Huisman's samples was within a large range while the crystallinity of our yarns is relatively high and fluctuates in a small range. For PET fibers with high and comparable crystallinity, amorphous orientation appears to be more important in governing thermal shrinkage than the fraction of amorphous regions.

Dimensional Stability. Dimensional stability is a very important characteristic when PET industrial yarns are used as reinforcement in radial tires. The unique structures such as high amorphous orientation, small long period and large numbers of small crystal grains, make HMLS yarn the best dimensional stability (small part load elongation and shrinkage) and highest initial modulus. SAXS data suggest that the tilting angle of the crystalline lamellae of HMLS yarn is the smallest, which may also be one of the reasons for the good dimensional stability. Aligning the molecules before drawing process and then crystallizing them with a high degree of crystallite orientation and small tilting angle give the best dimensional stability of HMLS yarn.[30] Conversely, aligning the molecules in the drawing process results in HT yarns with large long period and large tilting angle, which may destroy the dimensional stability.

Based on the above discussion, a brief presentation was summarized to show the key structural parameters, the mainly related process conditions as well as the related properties of PET industrial yarns, as shown in Table V. In this case, we focus on the general process–structure–property relationships of PET industrial yarns, rather than limit to the range of the four yarns studied in this paper. From Table V, it is clear that each structural characteristic was not simply controlled by a single process parameter and a series of process conditions should be applied to obtain a yarn with specific structures, i.e., amorphous orientation, crystal grain number, and long period. Compared with other structural characteristics, amorphous orientation has more influence on the mechanical properties and shrinkage. In addition, crystal grain number and long period also have an influence on the initial modulus and elongation (part load elongation and ultimate elongation) to some extent, respectively. Small tilting angle of lamellae may be a structure characteristic with respect to dimensional stability.

CONCLUSIONS

In this study, we re-examined the process–structure–property relationships of PET industrial yarns mainly using synchrotron radiation WAXD and SAXS. The four typical PET industrial yarns produced at different process conditions exhibit different structures and properties. Compared with other structural parameters, amorphous orientation is the most important structural characteristic in determining tenacity, initial modulus, part load elongation, ultimate elongation, and shrinkage. In addition, the crystal grain number appears to have an effect on the initial modulus, while the long period influences the elongation of PET yarns to some extent. A series of process condition parameters, such as spinning speed, draw ratio, and heat-setting temperatures, should be applied to produce yarns with unique structures and specific properties. The comprehensive understanding of the process–structure–property relationships may be helpful to develop new types of PET industrial yarns with desired properties.

ACKNOWLEDGMENTS

This work was supported by the China Postdoctoral Science Foundation (2014M55129). The authors acknowledge BL16B1 and BL15U1 beamlines in SSRF for SAXS and WAXD measurements. The authors express thanks to Mr. Hui Pan and Mr. Chao Zhang for valuable discussions.

REFERENCES

1. Gupta, V. B.; Ramesh, C.; Gupta, A. K. *J. Appl. Polym. Sci.* **1984**, *29*, 3727.
2. Gupta, V. B.; Ramesh, C.; Gupta, A. K. *J. Appl. Polym. Sci.* **1984**, *29*, 3115.
3. Hsieh, Y.-L.; Mo, Z. *J. Appl. Polym. Sci.* **1987**, *33*, 1479.
4. Huisman, R.; Heuvel, H. M. *J. Appl. Polym. Sci.* **1989**, *37*, 595.
5. Cruz, C. S.; Stribeck, N.; Zachmann, H. G.; Calleja, F. J. B. *Macromolecules* **1991**, *24*, 5980.
6. Calleja, F. J. B.; Cruz, C. S.; Asano, T. *J. Polym. Sci. Polym. Phys.* **1993**, *31*, 557.
7. Hirahata, H.; Seifert, S.; Zachmann, H. G.; Yabuki, K. *Polymer* **1996**, *37*, 5131.

8. Koncke, U.; Zachmann, H. G.; Balta Calleja, F. J. *Macromolecules* **1996**, *29*, 6019.
9. Murthy, N. S.; Bednarczyk, C.; Rim, P. B.; Nelson, C. J. *J. Appl. Polym. Sci.* **1997**, *64*, 1363.
10. Stribeck, N.; Zachmann, H. G.; Bayer, R. K.; Calleja, F. J. B. *J. Mater. Sci.* **1997**, *32*, 1639.
11. Asano, T.; Calleja, F. J. B.; Flores, A.; Tanigaki, M.; Mina, M. F.; Sawatari, C.; Itagaki, H.; Takahashi, H.; Hatta, I. *Polymer* **1999**, *40*, 6475.
12. Kawakami, D.; Ran, S. F.; Burger, C.; Fu, B.; Sics, I.; Chu, B.; Hsiao, B. S. *Macromolecules* **2003**, *36*, 9275.
13. Lv, J.; Wang, S. *J. Appl. Polym. Sci.* **2005**, *95*, 859.
14. Yamaguchi, T.; Komoriyama, K.; Ohkoshi, Y.; Urakawa, H.; Gotoh, Y.; Terasawa, N.; Nagura, M.; Kajiwara, K. *J. Polym. Sci. Polym. Phys.* **2005**, *43*, 1090.
15. Shioya, M.; Kawazoe, T.; Kojima, J.; Sakurai, S.; Yamamoto, K.; Kikutani, T. *Polymer* **2006**, *47*, 3616.
16. Huang, L.; Pan, L.; Inoue, T. *J. Appl. Polym. Sci.* **2007**, *104*, 787.
17. Uchiyama, T.; Suyama, M.; Alam, M. M.; Asano, T.; Henning, S.; Flores, A.; Calleja, F. J. B.; Mina, M. F. *Polymer* **2007**, *48*, 542.
18. Youssefi, M.; Morshed, M.; Kish, M. H. *J. Appl. Polym. Sci.* **2007**, *106*, 2703.
19. Shioya, M.; Kawazoe, T.; Okazaki, R.; Suei, T.; Sakurai, S.; Yamamoto, K.; Kikutani, T. *Macromolecules* **2008**, *41*, 4758.
20. Slobodian, P. *J. Therm. Anal. Calorim.* **2008**, *94*, 545.
21. Hahm, W. G.; Takarada, W.; Ito, H.; Kikutani, T. *Int. Polym. Process.* **2009**, *24*, 280.
22. Okada, K.; Higashioji, T.; Nakagawa, T.; Uchida, H.; Takahashi, K.; Inoue, R.; Nishida, K.; Kanaya, T. *Polym. J.* **2013**, *45*, 50.
23. Samui, B. K.; Prakasan, M. P.; Ramesh, C.; Chakrabarty, D.; Mukhopadhyay, R. *J. Text. I* **2013**, *104*, 35.
24. Rim, P. B.; Nelson, C. J. *J. Appl. Polym. Sci.* **1991**, *42*, 1807.
25. Wang, Y.; Gao, L.; Wang, X.; Zhang, Y.; Wang, H. *Adv. Mater. Res.* **2012**, *560–561*, 614.
26. Wang, X.; Wang, Y.; Pan, Q.; Zhang, Y.; Wang, H. *Synth. Fiber Indus.* **2012**, *35*, 35.
27. Wang, X.; Tian, F.; Zhang, Y.; Wang, H. *Adv. Mater. Res.* **2011**, *332–334*, 313.
28. Canetti, M.; Bertini, F. *Eur. Polym. J.* **2010**, *46*, 270.
29. Sujica, M. Z.; Smole, M. S. *J. Appl. Polym. Sci.* **2003**, *89*, 3383.
30. Murthy, N. S.; Grubb, D. T. *J. Polym. Sci. Polym. Phys.* **2003**, *41*, 1538.
31. Cho, D. H.; Yu, W.-R.; Youk, J. H.; Yoo, J. H. *Eur. Polym. J.* **2007**, *43*, 3562.
32. Ramesh, C.; Gupta, V. B.; Radhakrishnan, J. *J. Macromol. Sci. Phys.* **1997**, *B36*, 281.
33. Rastogi, R.; Vellinga, W. P.; Rastogi, S.; Schick, C.; Meijer, H. E. H. *J. Polym. Sci. Polym. Phys.* **2004**, *42*, 2092.
34. Verma, R. K.; Hsiao, B. S. *Trends in Polymer Science* **1996**, *4*, 312.
35. Denchev, Z.; Nogales, A.; Sics, I.; Ezquerra, T. A.; Balta-Calleja, F. J. *J. Polym. Sci. Polym. Phys.* **2001**, *39*, 881.
36. Murthy, N. S.; Grubb, D. T.; Zero, K.; Nelson, C. J.; Chen, G. *J. Appl. Polym. Sci.* **1998**, *70*, 2527.
37. Fu, Y. G.; Annis, B.; Boller, A.; Jin, Y. M.; Wunderlich, B. *J. Polym. Sci. Polym. Phys.* **1994**, *32*, 2289.
38. Abbasi, M.; Mojtahedi, M. R. M.; Khosroshahi, A. *J. Appl. Polym. Sci.* **2007**, *103*, 3972.
39. Kolb, R.; Seifert, S.; Stribeck, N.; Zachmann, H. G. *Polymer* **2000**, *41*, 2931.
40. Peng, K. L.; Roland, C. M. *J. Polym. Sci. Polym. Phys.* **1993**, *31*, 1339.
41. Kiang, C. T.; Cuculo, J. A. *J. Appl. Polym. Sci.* **1992**, *46*, 83.
42. Kawakami, D.; Burger, C.; Ran, S.; Avila-Orta, C.; Sics, I.; Chu, B.; Chiao, S.-M.; Hsiao, B. S.; Kikutani, T. *Macromolecules* **2008**, *41*, 2859.
43. Wang, Z. G.; Hsiao, B. S.; Fu, B. X.; Liu, L.; Yeh, F.; Sauer, B. B.; Chang, H.; Schultz, J. M. *Polymer* **2000**, *41*, 1791.
44. Murthy, N. S.; Correale, S. T.; Minor, H. *Macromolecules* **1991**, *24*, 1185.
45. Alexander, L. E. X-Ray Diffraction Methods in Polymer Science; Wiley-Interscience: New York, **1969**, p 137.
46. Gupta, V. B.; Kumar, S. *Text. Res. J.* **1979**, *49*, 405.
47. Tang, Y. J.; Jiang, Z. Y.; Men, Y. F.; An, L. J.; Enderle, H. F.; Lilge, D.; Roth, S. V.; Gehrke, R.; Rieger, J. *Polymer* **2007**, *48*, 5125.
48. Wen, H.; Jiang, S.; Men, Y.; Zhang, X.; An, L.; Wu, Z.; Okuda, H. *J. Chem. Phys.* **2009**, *130*, 164909.
49. Murthy, N. S.; Bednarczyk, C.; Moore, R. A. F.; Grubb, D. T. *J. Polym. Sci. Polym. Phys.* **1996**, *34*, 821.
50. Men, Y. F.; Rieger, J.; Lindner, P.; Enderle, H. F.; Lilge, D.; Kristen, M. O.; Mihan, S.; Jiang, S. C. *J. Phys. Chem. B* **2005**, *109*, 16650.
51. Hsiao, B. S.; Verma, R. K. *J. Synchrotron. Radiat.* **1998**, *5*, 23.
52. Stribeck, N. *J. Appl. Crystallogr.* **2001**, *34*, 496.
53. Stribeck, N.; Fakirov, S. *Macromolecules* **2001**, *34*, 7758.
54. Moseley, W. W. *J. Appl. Polym. Sci.* **1960**, *3*, 266.
55. Dumbleton, J. H. *J. Polym. Sci. Polym. Phys.* **1968**, *6*, 795.
56. Samuels, R. J. *J. Polym. Sci. Polym. Chem.* **1965**, *3*, 1741.
57. Murthy, N. S.; Grubb, D. T. *J. Polym. Sci. Polym. Phys.* **2006**, *44*, 1277.
58. Heuvel, H. M.; Lucas, L. J.; Vandenheuvel, C. J. M.; Deweijer, A. P. *J. Appl. Polym. Sci.* **1992**, *45*, 1649.